Korean J. Chem. Eng., 36(5), 828-836 (2019)
DOI: 10.1007/s11814-019-0252-8

pISSN: 0256-1115
eISSN: 1975-7220

Rheological and mechanical properties of PMMA/organoclay nanocomposites prepared via ultrasound-assisted in-situ emulsion polymerization

Maneesh Kumar Poddar*, Kavita Vishwakarma, and Vijayanand Suryakant Moholkar*,†**

*Department of Chemical Engineering, Indian Institute of Technology Guwahati, Guwahati - 781039, Assam, India
**Department of Physics, Indian Institute of Technology Patna, Patna - 801103, Bihar, India
(*Received 5 December 2018 • accepted 5 March 2019*)

Abstract–This study investigated the rheological and mechanical properties of PMMA/organically modified Cloisite 30B nanocomposites (clay loading 1-5 wt%) synthesized via ultrasound-assisted in-situ emulsion polymerization. XRD patterns and TEM micrographs of the nanocomposites confirm complete exfoliation and uniform distribution of nanoclay platelets in host poly(methyl methacrylate) matrix. As a consequence, the nanocomposites synthesized with sonication were found to have superior properties as compared to the nanocomposites synthesized with mechanical stirring. Measurement of rheological properties using melt rheology revealed that magnitudes of storage modulus, loss modulus and complex viscosity increased with incorporation of clay platelets in polymer matrix due to the flow restriction of PMMA chains induced by nanofiller. Analysis of mechanical properties of nanocomposites showed maximum Young's modulus of 1.8 GPa with weight average molecular weight (M_w) of 581,130 g mol^{-1} for 2 wt% clay loading. The enhancements in rheological and mechanical properties of nanocomposites are attributed to the physical and chemical effect of ultrasound and cavitation, i.e. generation of intense microturbulence and free radicals in the emulsion polymerization reaction system.

Keywords: PMMA, Organoclay, Nanocomposite, Melt Rheology, Ultrasound, Cavitation

INTRODUCTION

Polymer-layered silicate nanocomposites have emerged as special class of materials due to their distinct physical and chemical properties [1-7]. Among various clay silicates used for nanocomposite synthesis, Cloisite 30B clay, which belongs to smectites family, has attracted special interest due to its high aspect ratio (1 : 1,000) and large inter-gallery spacing (*d*-spacing) between the clay layers [8,9]. As per published literature, incorporation of Cloisite 30B clay in the host polymer matrix significantly improves the mechanical, thermal and barrier properties of pristine PMMA [10,11]. Previous authors have reported various techniques, such as in-situ emulsion polymerization, bulk polymerization, suspension polymerization, solvent blending method and melt intercalation for the preparation of silicate based PMMA/clay nanocomposites [12-17]. Among these, in situ emulsion polymerization is the most widely used technique due to its simple procedure and other merits such as use of water as a heat controlling medium during polymerization. However, the conventional protocol of in-situ emulsion polymerization with mechanical stirring cannot achieve widening of the clay galleries or *d*-spacing. This results in intercalated or semi-exfoliated structure of the nanocomposites with formation of clay agglomerates in the host polymer matrix [18-20].

More recently, the technique of ultrasound-assisted synthesis of polymer nanocomposites has received special attention due to high encapsulation and uniform dispersion of nanofiller in the monomer droplets [21-26]. Application of sonication during polymer nanocomposite synthesis has proven beneficial due to the physical and chemical effects of ultrasound and cavitation. Physical effect of ultrasound involves generation of intense energy concentration in the form of microturbulence and shock waves on extremely small temporal and spatial scale, which can generate fine emulsion between aqueous and organic phase with uniform distribution of nanofiller in the polymer matrix. Chemical effect of sonication involves generation of free radicals ($^{\bullet}H$, $^{\bullet}OH$) by thermal decomposition of water vapor and gas molecules existing in the bubble during transient collapse [17,27-29]. Transient collapse of cavitation bubbles produces extremely high temperatures and pressures (~5,000 K, ~1,000 atm) with a rapid heating/cooling rate (>10^{10} K/s) in very short duration of time (~50 ns) [30-32]. At this extreme condition, the cavitation bubble may get fragmented at the point of maximum compression with release of the chemical species inside it into the bulk liquid. These species are responsible for inducing/accelerating chemical reactions such as polymerization. In the context of synthesis of polymer nanocomposites, both physical and chemical effects of ultrasound and cavitation are relevant.

Among various acrylic polymers used for the synthesis of nanocomposites, polymethyl methacrylate (PMMA) is an important thermoplastic by virtue of its high optical transparency and thermal stability. Conventional techniques of PMMA/clay nanocomposite synthesis (at moderate to high nanofiller loading) have poor mechanical properties such as low Young's modulus of elasticity, low bulk and storage modulus and low molecular weight [33,34]. Recently, Kumar et al. [34] synthesized PMMA/clay nanocomposites using

†To whom correspondence should be addressed.
E-mail: vmoholkar@iitg.ac.in

melt intercalation techniques in addition to maleic anhydride as a compatibilizer. In this study, Kumar et al. [34] reported the effect of compatibilizer on the rheological properties of nanocomposites. However, a comprehensive investigation of mechanical and rheological properties of PMMA/Cloisite 30B nanocomposites synthesized via ultrasound-assisted in-situ emulsion polymerization has not been reported. A previous paper has reported rheological properties of PMMA/clay nanocomposites synthesized using bulk polymerization and melt-mixing with sonication [35]. However, due to high viscosity of polymer solution, these techniques have difficulties in controlling the polymerization rate. Therefore, synthesis of polymer nanocomposites using ultrasound-assisted emulsion polymerization could be a preferential method for simultaneous control of polymerization rate with maximum encapsulation and uniform dispersion of nanoclay in the polymer matrix.

In the present contribution, we report investigation of rheological and mechanical properties of PMMA/Cloisite 30B nanocomposites synthesized via ultrasound-assisted in-situ emulsion polymerization. In addition, we have also synthesized nanocomposites with conventional mechanical stirring to demonstrate efficacy of sonication in achieving uniform distribution of silicates layer into the PMMA chain matrix that contribute towards enhancement of physical properties.

EXPERIMENTAL

1. Materials

Monomer methyl methacrylate (MMA, purity: 98.5% AR grade) was obtained from Hi-Media India Ltd. The organic inhibitor hydroquinone present in monomer was separated through a bed of neutral alumina oxide powder via adsorption. The organo-modified Cloisite 30B clay was purchased from Southern Clay Products, Inc. (USA). The organic solvent, dichloromethane (DCM, at a purity of 99.5%), was purchased from SRL, India. The inorganic initiator potassium persulfate ($K_2S_2O_8$, AR grade) and the surfactant, sodium dodecyl sulfate (SDS), were obtained from Merck India Ltd. Millipore water was used as the reaction medium in all experiments.

2. Preparation of Polymer Nanocomposite

Neat PMMA and PMMA/Cloisite 30B nanocomposites were synthesized as per protocol reported in our previous work [10]. Briefly, 15.0 g of MMA (methyl methacrylate) with 0.75 g of KPS (potassium persulfate) in addition with 0.87 g SDS (sodium dodecyl sulfonate) with different loadings of Cloisite 30B clay (1, 2 and 5 wt%) were mixed in 45 mL Millipore water in a jacketed glass reactor. This mixture was sonicated for 30 s for fine emulsification. Next, temperature of reaction mixture was raised to 65±2 °C with continuous circulation of hot water in the reactor jacket. After achieving the polymerization temperature (65±2 °C), the in-situ emulsion polymerization was conducted with application of ultrasound irradiation (or sonication) for the next 1 h. Sonication of the reaction mixture at frequency of 20 kHz was carried out using a microprocessor-controlled probe type sonicator. Theoretical power input to the probe was 200 W, which corresponded to acoustic pressure amplitude of ~2 bar, as per calorimetric measurements. The overall polymerization mechanism for the synthesis of PMMA/Cloisite 30B nanocomposites was involved in two steps and is depicted in Fig. 1. In the first step, the stacked clay layers showed enhancement in interlayer clay spacing (*d*-spacing) after the sonication due to the

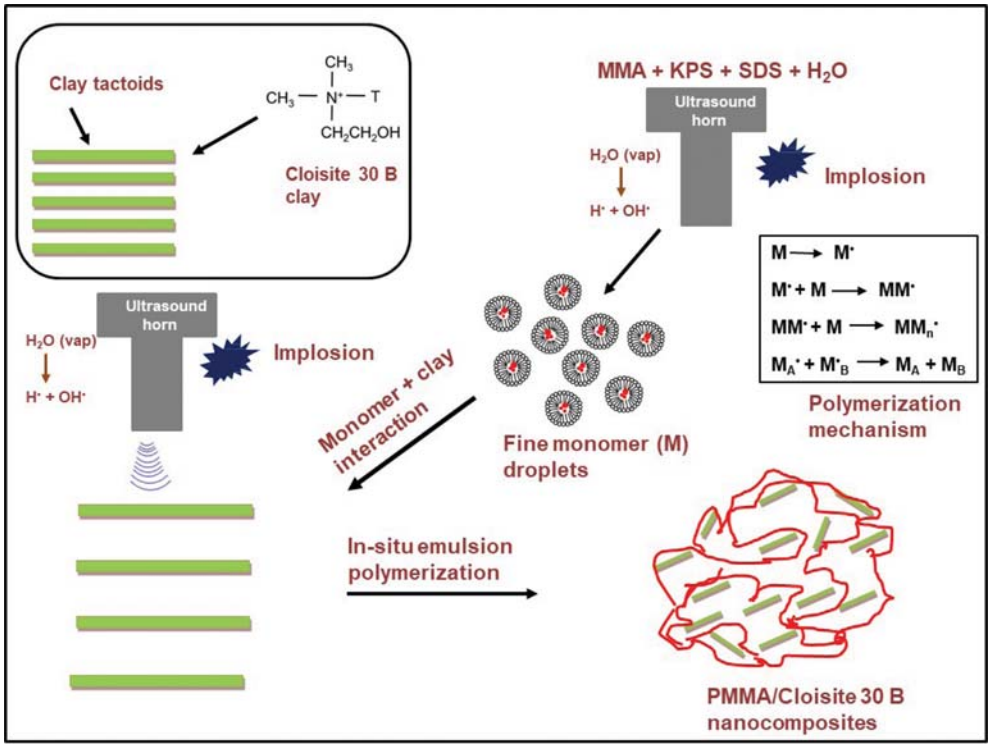

Fig. 1.A schematic diagram of the mechanism of PMMA/Cloisite 30B nanocomposite synthesis induced by ultrasound assisted in-situ emulsion polymerization.

intense microtubulence generated by ultrasound and cavitation. While in the second step, the free radicals generated by the combined effects of ultrasound ($H^{\bullet}$ or $OH^{\bullet}$) and inorganic initiator potassium persulfate ($SO_4^{\bullet-}$) initiated the polymerization reaction via converting monomer M into $M^{\bullet}$ monomer radicals [7,10]. These radicals were transported towards the micelles formed in the presence of surfactants (SDS) above its critical micelles concentration (CMC). The nanoscale emulsion or fine dispersion generated by ultrasound in the form of micro-convection accelerated the monomer and radical interaction with already exfoliated clay structure and propagated the in-situ synthesis of PMMA/clay nanocomposites by ultrasound sound assisted method. After completion of the polymerization, the unconverted monomer and moisture were removed by evaporation inside a vacuum oven for 15 h at 65 °C. The remaining surfactants present in the dried latex sample were removed through several water washes. The resulting nanocomposites free of anionic surfactants were further vacuum dried. The final dried latex nanocomposites were used for making the thin film of PMMA/Cloisite 30B. Thin films of nanocomposites (thickness ~0.2 mm) were prepared after dispersing the final latex nanoparticles into the organic solution of dichloromethane. After evaporation of the solvent, the final dried PMMA/Cloisite 30B nanocomposites were used for characterization.

2-1. Control Experiments

To evaluate the efficacy of sonication in enhancing the properties of the nanocomposites, control experiments were performed using mechanical stirring of the reaction mixture during in-situ emulsion polymerization. The protocol in control experiments was exactly the same as the ultrasound-assisted experiments, except that reaction mixture was continuously stirred at 600 rpm using a magnetic bar. Loading of nanoclay in the control experiments was restricted to only 1.0 and 2.0 wt%. Higher clay loading in mechanical stirring based control experiments is prone to heavy clay agglomeration into the polymer matrix, which further decreases the nanocomposite properties. Therefore, control experiments were carried out at lower clay loading of 1 and 2 wt%. Nanocomposites obtained in the control experiments were also characterized for rheological and mechanical properties. The morphological structure of these nanocomposites was analyzed by transmission electron microscopy (TEM).

3. Characterization of PMMA/Cloisite 30B Nanocomposites

3-1. X-ray Diffraction

The interlayer *d*-spacing of organically modified Cloisite 30B nanoclay and PMMA/clay nanocomposites was calculated using X-ray diffraction patterns (XRD). XRD analysis was performed using D8 Advance fully automatic X-ray diffractometer (Make: Bruker, Model: D8 Advance) equipped with a Cu-Kα radiation (λ= 0.15418 nm) and Ni filter in an air atmosphere. The pattern was set for 2 range of 1° to 50° with a scan rate of 0.05° s^{-1}.

3-2. Optical Transparency

Optical transparency of film of dimensions 20 mm×20 mm with 0.3 mm thickness of neat PMMA and PMMA/Cloisite 30B nanocomposites was done by using UV-Vis spectrometer (Perkin Elmer) in visible light wavelength of 400-800 nm.

3-3. Rheological Measurement

The melt rheological experiments of pristine PMMA and PMMA/Cloisite 30B were conducted using a rheometer (Anton Paar MCR101) equipped with parallel plate geometry in an oscillatory shear mode with 1% strain at 240 °C. The analysis involved using a film sample with the thickness of 1.5 mm and diameter of 25 mm.

3-4. Mechanical Properties

Mechanical properties such as tensile strength, Young's modulus and percentage elongation were determined using the Universal Testing Machine (INSTRON 8801, UK). For analysis of mechanical properties, a rectangular film of nanocomposite with a size of 100 mm×25 mm with the film thickness of 0.4 mm was prepared according to ASTM D882 with a standard gauge length of 50 mm with the cross head speed of 0.5 mm/min.

3-5. Transmission Electron Microscopy

Transmission electron microscopy (Make: JEOL, Model: JEM 2100) was used for analyzing the surface and morphological structure of PMMA/Cloisite 30B nanocomposites.

3-6. Gel Permeation Chromatography

Analysis of molecular weight of neat PMMA and its nanocom-

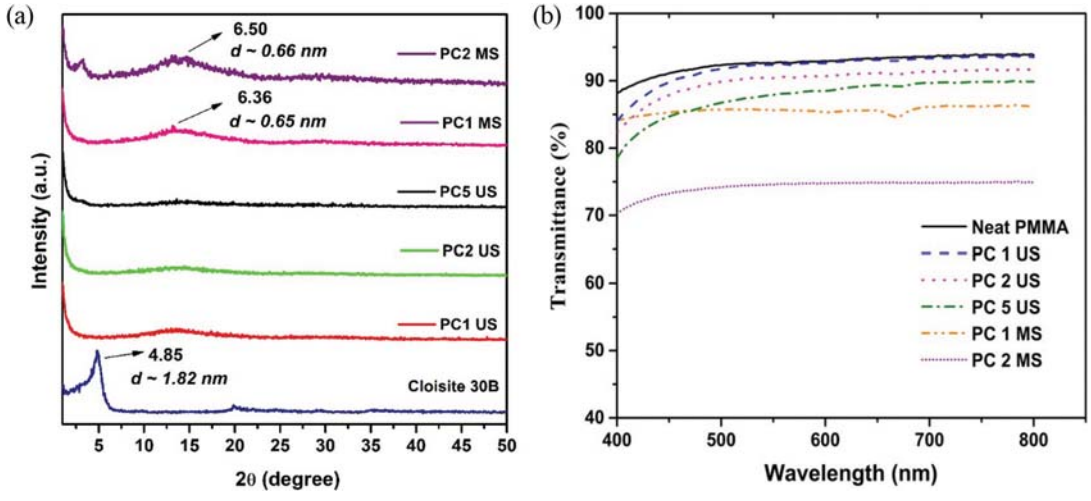

Fig. 2. (a) XRD patterns and (b) optical transparency of PMMA/Cloisite 30B nanocomposites synthesized with various loading of Cloisite 30B clay using ultrasound (US) and mechanical stirring (MS).

posites of PMMA/Cloisite 30B clay was determined using gel permeation chromatography (GPC) (Make: Shimadzu, Model: LC solutions) with chloroform as the eluent.

RESULT AND DISCUSSION

1. XRD Analysis

XRD patterns of pristine Cloisite 30B nanoclay and the PMMA/Cloisite 30B nanocomposites for different nanofiller loadings are shown in Fig. 2(a). It is evident that pristine Cloisite 30B exhibits a sharp diffraction peak at 2θ=4.85° corresponding to interlayer gallery spacing or *d*-spacing (0 0 1) of 1.82 nm. The interlayer d spacing was calculated according to Bragg's law d=λ/2sinθ, where d is the interplanar distance, θ is the diffraction angle and λ is the wavelength of incident X-ray. The nanocomposites synthesized using sonication showed absence of any diffraction peak for all clay loading of 1, 2 and 5 wt%. This clearly indicates complete exfoliation of clay layers into the bulk PMMA matrix during in-situ polymerization. High shear force and intense microturbulence generated in the reaction mixture during sonication could effectively de-laminate the individual silicate layers into single platelets, which can get entrapped and disperse into the monomer (MMA) droplets. During emulsion polymerization, the OH group of SDS surfactant adsorbed at the edge of organo-modified (O-MMT) clay can interact with polar group of MMA monomer. The radicals formed during collapse of transient cavitation bubbles and dissociation of inorganic initiator (KPS) can react with monomer at the cavitation bubble/solution interface with increase in polymerization rate. In the control experiments, interlayer *d*-spacing of the nanocomposites synthesized with mechanically stirring (MS) was obtained as 0.65 and 0.66 nm at 2θ=6.36° and 6.50° for 1 and 2 wt% clay loading, respectively. Convection generated through mechanical stirring at 600 rpm is unable to de-laminate the clay platelets into individual layers (due to absence of high energy shear), and thus results in intercalated structure.

2. Optical Transparency

The results of optical transparency of neat PMMA and PMMA/Cloisite 30B nanocomposites with various clay loadings are depicted in Fig. 2(b). The neat PMMA showed high optical transparency of more than 85% in the visible light range. The addition of nanoclay lowered the optical transparency due to the absorption of visible light in the presence of clay nanosheets. However, the reduction in optical transparency of PMMA/Cloisite 30B nanocomposites synthesized with sonication was observed minimum as compared to the optical transparency of nanocomposites synthesized via conventional based mechanical stirring. High optical transparency of PMMA/Cloisite 30B nanocomposites synthesized via sonication attributed to the uniform distribution and exfoliated structure of nano clay into the base PMMA matrix.

3. Rheological Studies

The results of melt rheological measurements of neat PMMA and PMMA/Cloisite 30B nanocomposites are shown in Figs. 3-6. Since rheological measurement is highly sensitive to the amount of nanofiller loadings and its types, an oscillatory measurement is always preferred for analysis of dynamic rheological properties of polymer nanocomposites. Results of three rheological properties,

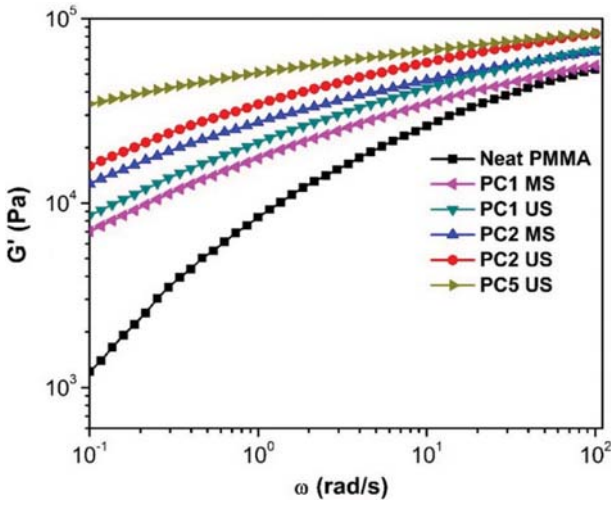

Fig. 3. Storage modulus of neat PMMA and PMMA/Cloisite 30B nanocomposites synthesized with various loading of Cloisite 30B clay using ultrasound (US) and mechanical stirring (MS).

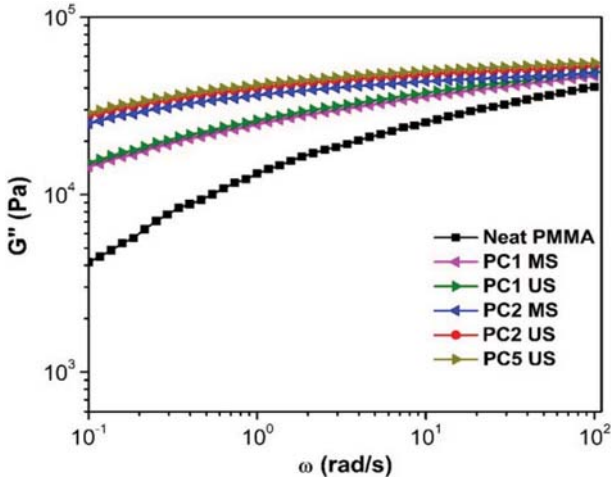

Fig. 4. Loss modulus of neat PMMA and PMMA/Cloisite 30B nanocomposites synthesized with various loading of Cloisite 30B clay using ultrasound (US) and mechanical stirring (MS).

storage modulus (G′), loss modulus (G″) and complex viscosity (η^*), are presented in the range of angular frequencies of 0.1-100 rad/s. As shown in Figs. 3 and 4, the magnitude of storage (G′) and loss modulus (G″) of PMMA/Cloisite 30B nanocomposites were significantly higher as compared to pristine PMMA. G′ and G″ values, which essentially represent viscoelastic properties of the polymer, are highly sensitive at low frequencies. At low frequency ($\sim\omega<$ 10), both modulus G′ and G″ demonstrated weak frequency dependence, and also showed a gradual change in behavior from liquid-like [$G'\propto\omega$, $G''\propto\omega^2$] to solid-like with increasing clay loading. This phenomenon can be attributed to the retardation of molecular relaxation processes induced by the confined geometric effect [36,37]. However, at high frequency ($\sim\omega>10$) the viscoelastic properties for all clay loading show almost similar behavior. For low frequency range, the relaxation time period of polymer chains is the longest, which results in high magnitude of storage modulus G′ with encap-

sulation of nanofiller in polymer matrix. Incorporation of the clay material in polymer matrix affects the relaxation time period of polymeric segmental chain motion and provides stiffness to the polymer matrix. At higher frequencies, the effect of clay on the long range motions of the polymer chains decreases, and the trends of G′ and G″ versus frequency for nanocomposites overlap closely with different clay loadings. As shown in Figs. 3 and 4, at low frequency values, the nanocomposites of PMMA/Cloisite 30B synthesized with sonication (PC1 US, PC2 US and PC5 US) showed significantly higher values of G′ and G″, as compared to nanocomposites synthesized with mechanical stirring (PC1 MS and PC2 MS). An explanation for marked rise in G′ and G″ with addition of clay can be given in terms of increase in relaxation time and higher confinement of polymer chain within the clay platelets uniformly distributed in the polymer matrix due to sonication. Microconvection generated during sonication causes nanoscale dispersion of clay platelets in bulk PMMA matrix, which improves the compatibility between the exfoliated clay layers with PMMA matrix. Sonication of reaction mixture also results in greater encapsulation of the nanofiller in the polymer matrix. On the other hand, agitation provided by mechanical stirring is insufficient in achieving high encapsulation and uniform distribution of the nanoclay in the PMMA matrix during emulsion polymerization.

Fig. 5 explains the stress relaxation behavior of neat PMMA and PMMA/Cloisite 30B nanocomposites in order to examine the change of nanocomposites to the solid like states. The stress relaxation behavior in which the stress relaxation modulus (G(t)) was calculated from the numerical value of G′(ω) and G″(ω) in Figs. 3 and 4 using Schwarzl equation [38] as given below:

$$G(t) \cong G'(\omega) - 0.560G''(\omega/2) + 0.200G''(\omega) \quad (1)$$

The Schwarzl Eq. (1) can predict the short-term relaxation behavior of material and is helpful in confirming the solid-like behavior of nanocomposites [39,40]. Fig. 5 confirms an increase in the relaxation modulus G(t) with increase in clay loading. However, the

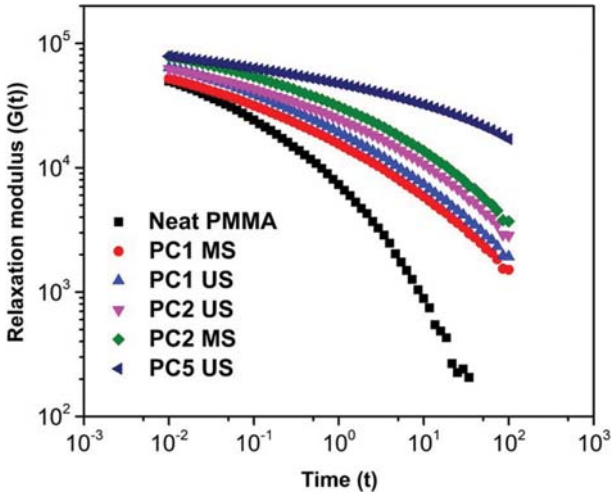

Fig. 5. Relaxation modulus (G(t)) of neat PMMA and PMMA/Cloisite 30B nanocomposites synthesized with various loading of Cloisite 30B clay using ultrasound (US) and mechanical stirring (MS) (calculated using G′(ω) and G″(ω)).

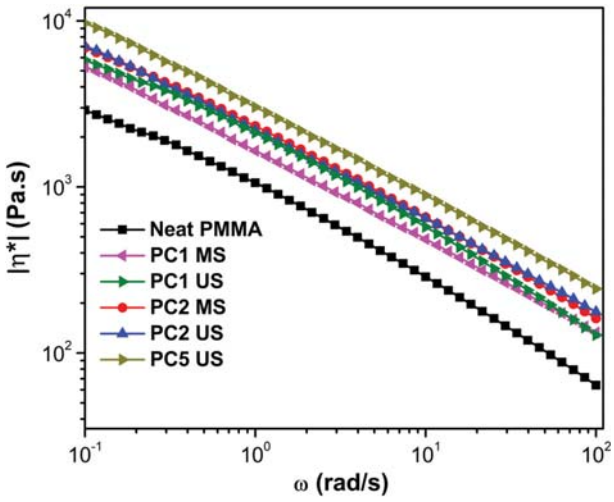

Fig. 6. Complex viscosity of neat PMMA and PMMA/Cloisite 30B nanocomposites synthesized with various loading of Cloisite 30B clay using ultrasound (US) and mechanical stirring (MS).

increase in relaxation modulus G(t) is higher for sonochemical synthesized PMMA/Cloisite 30B nanocomposites as compared to the mechanical stirring for similar clay loading. This increase in G(t) signifies a strong interaction between silicate layers and polymer matrix due to exfoliated structure of PMMA/Cloisite 30B nanocomposites, which further provides long relaxation time of resulting nanocomposites synthesized using sonochemical methods.

Variations in complex viscosity (η^*) of neat PMMA and PMMA/Cloisite 30B with frequency are depicted in Fig. 6. These trends are almost similar to the trends in G′ and G″. Incorporation of nanoclay in PMMA matrix increases the viscosity of PMMA/clay nanocomposites as compared to the neat PMMA. Rise in the viscosity was proportionate to the clay loading. Moreover, for a particular clay loading, higher rise in viscosity was observed for nanocomposites synthesized in ultrasound-assisted emulsion polymerization, as compared to the nanocomposites synthesized with mechanical stirring. The enhancement in viscosity is attributed to flow restriction of polymer chain in the molten state due to increase in loading of nanoparticle in polymer matrix [39,41,42]. As noted earlier, application of sonication during emulsion polymerization causes uniform distribution of nanoclay in the polymer matrix, with widening of the galleries of clay layers. This can increase the intermolecular interaction between clay platelets and bulk PMMA matrix, which is essentially manifested in terms of enhanced flow restriction between bulk polymer chains, and thus, enhanced viscosity [22,43].

4. Mechanical Properties

Mechanical properties of as-synthesised neat PMMA and PMMA/Cloisite 30B nanocomposites are shown in Figs. 7-9. The tensile strength of pristine PMMA is 32.74 MPa. With addition of clay to polymer matrix (1, 2, and 5 wt%), the resulting nanocomposites reveal reduction in the tensile strength. The reduction in tensile strength of PMMA with addition of clay is attributed to the amorphous and brittle structure of PMMA. The brittle structure of PMMA can further increase, which the loading of nanoclay due to its stiff structure and further decreases the tensile strength of the

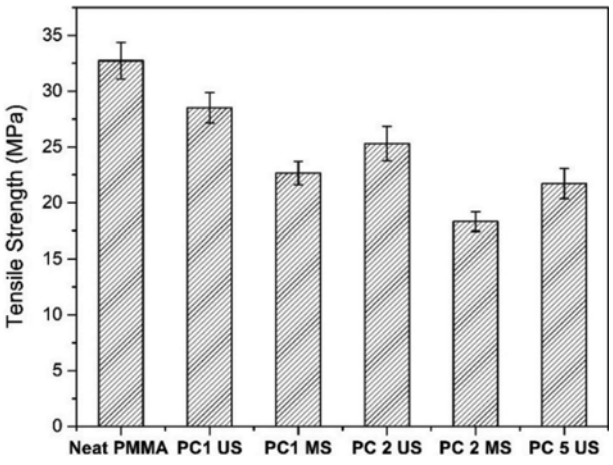

Fig. 7. Tensile strength of neat PMMA and PMMA/Cloisite 30B nanocomposites synthesized with various loading of Cloisite 30B clay using ultrasound (US) and mechanical stirring (MS).

nanocomposites. A similar trend of reduction in tensile strength with increase in clay loading was reported by Kumar et al. [44]. In this study, the authors found a similar trend of reduction of tensile strength of PMMA/clay nanocomposites as compared to the neat PMMA using various compatibilizers. Neat PMMA itself has brittle character, which further increases with incorporation of clay in the polymer matrix. This is manifested in terms of reduction in tensile strength that varies in proportion of clay loading [44]. The tensile strength of nanocomposites synthesized with mechanical stirring with clay loading of 1 and 2 wt% is significantly smaller than the corresponding nanocomposites synthesized with ultrasound-assisted technique. This result is attributed to non-uniform dispersion and intercalated structure of clay platelets in bulk PMMA matrix, which can form agglomerates. These agglomerates can form centers of stress concentration, essentially weakening the overall structure.

Fig. 8 shows Young's modulus of PMMA/Cloisite 30B nanocomposites for different clay loadings. Variations in Young's modulus of nanocomposites show opposite trends as compared to the trends in tensile strength. Young's modulus of neat PMMA was 1.17 GPa. Nanocomposites synthesized with 1 and 2 wt% clay loading have higher Young's modulus of 1.4 and 1.7 GPa, respectively. The significant rise in Young's modulus is due to the presence of more neighboring sites of hydrogen molecules available in clay layers, which can further increase the nanocomposite stiffness during emulsion polymerization. The marked rise in stiffness can restrict the elastic deformation and make the nanocomposites more brittle. However, for the highest clay loading of 5 wt%, Young's modulus of nanocomposite reduces to 1.6 GPa. Yet again, this could be a consequence of non-uniform dispersion of silicate layers in bulk PMMA matrix that leads to an increase in agglomeration/segregation of the nanofiller. As noted earlier, the agglomerates form weak spots in the polymer matrix that act as locations of stress concentration, which could result in development and propagation of cracks. Young's modulus of nanocomposites synthesized with mechanical stirring is significantly less than those synthesized with sonication due to non-uniform distribution of silicate layers in polymer matrix.

Percentage elongations of pristine PMMA and PMMA/Cloisite 30B nanocomposites (1, 2 and 5 wt%) are shown in Fig. 9. The results clearly indicate that percentage strain at break continuously reduces with clay loading in polymer matrix. The percentage elongation in pristine PMMA was 3.92%. For 5 wt% clay loading, the nanocomposite showed least percentage elongation of merely 0.7%. Moreover, the percentage elongations of PMMA/Cloisite 30B nanocomposites for 1 and 2 wt% loading are smaller than the corresponding nanocomposites synthesized with sonication. Explanations to these trends can be given along similar lines as for the trends in tensile strength and Young's modulus.

5. TEM Characterization

TEM analysis of nanocomposites was performed to assess the dispersion of clay platelets in polymer matrix. Figs. 10(a) and (b) show TEM micrographs depicting structural morphology of PMMA/Cloisite 30B nanocomposites synthesized using sonication with clay loading of 1 and 2 wt%. The dark clay platelets seen in Figs. 10(a) and (b) indicate the intersection of individual clay layers, while

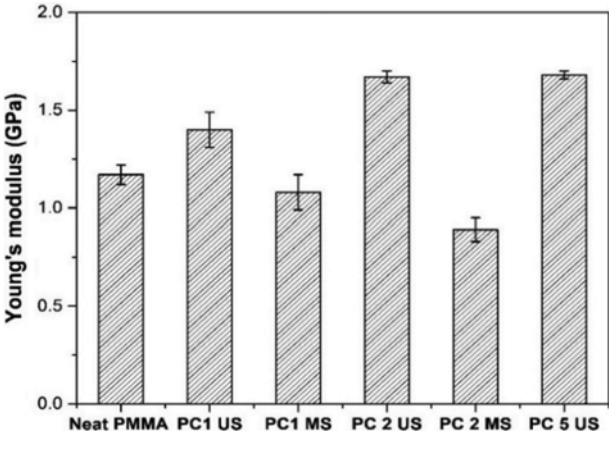

Fig. 8. Young's modulus of neat PMMA and PMMA/Cloisite 30B nanocomposites synthesized with various loading of Cloisite 30B clay using ultrasound (US) and mechanical stirring (MS).

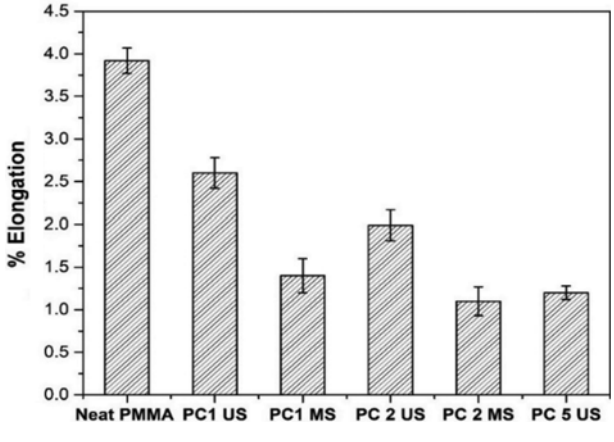

Fig. 9. Percentage elongation of neat PMMA and PMMA/Cloisite 30B nanocomposites synthesized with various loading of Cloisite 30B clay using ultrasound (US) and mechanical stirring (MS).

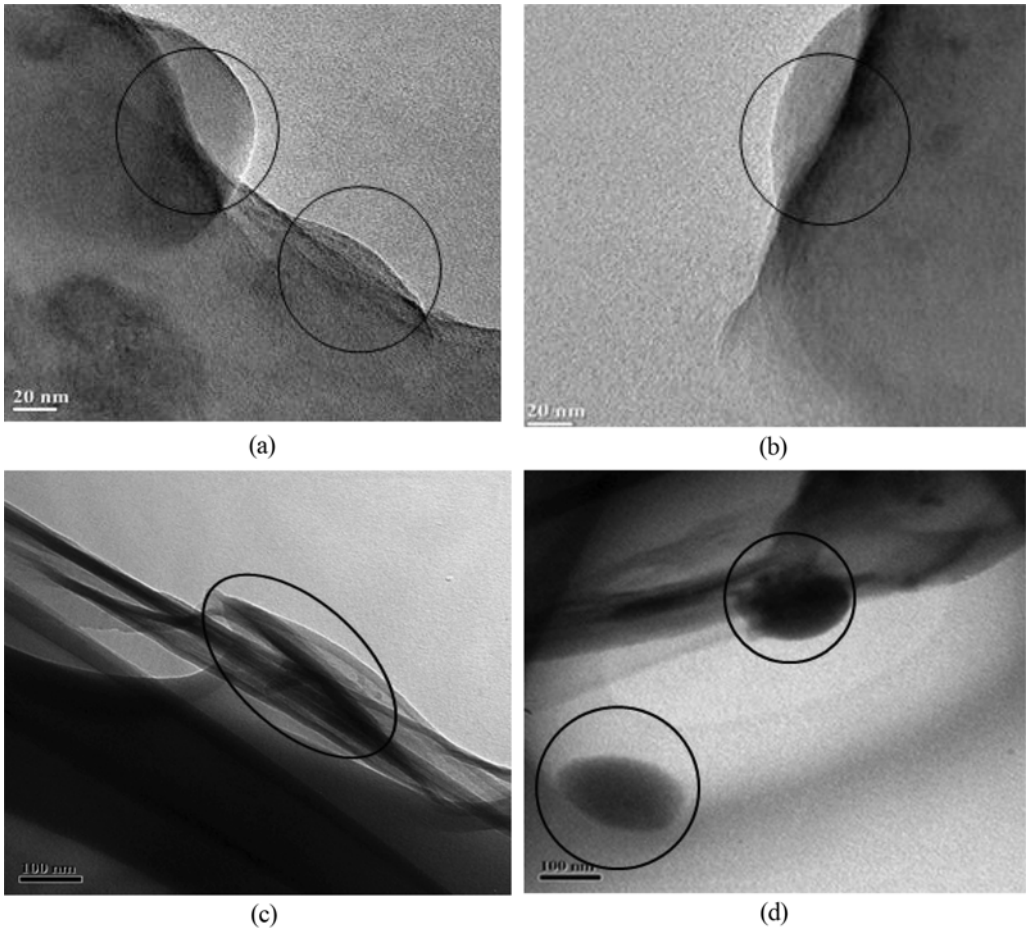

Fig. 10. TEM micrographs of PMMA/Cloisite 30B clay nanocomposites synthesized with various loading of Cloisite 30B clay with ultrasound (US) and mechanical stirring (MS). (a) 1 wt% US, (b) 2 wt% US, (c) 1 wt% MS and (d) 2 wt% MS.

the bright areas represent the bulk polymer phase. The results clearly indicate that individual dark platelets of clay layers are completely exfoliated and uniformly dispersed into the bulk polymer matrix. Some dark structures in Fig. 10(b) could be clay platelets that are closely spaced with each other with relatively random orientations. Figs. 10(c) and d show micrographs of nanocomposites synthesized via mechanical stirring with clay loading of 1 and 2 wt%. Agglomerates of nanofiller in the PMMA matrix are clearly evident from these micrographs. This is another evidence which suggests that strong microconvection generated by sonication not only causes complete exfoliation of the clay tactoids, but also disperses them uniformly into the polymer matrix. On the other hand, mechanical stirring cannot achieve either exfoliation or dispersion of clay tactoids in polymer matrix, resulting in nanocomposites with inferior properties.

6. Gel Permeation Chromatography

Molecular weights of neat PMMA and PMMA/Cloisite 30B nanocomposites are depicted in Table 1. The neat PMMA synthe-

Table 1. Results of the molecular weight analysis of neat PMMA and various loading of PMMA/Cloisite 30B clay nanocomposites

Name of sample	Weight average molecular weight (M_w) g mol^{-1}	Number average molecular weight (M_n) g mol^{-1}	Polydispersity (M_w/M_n)
Neat PMMA	435392	234301	1.86
PC 1 US	478506	210899	2.27
PC 1 MS	256372	172641	1.49
PC 2 US	581130	299454	1.94
PC 2 MS	228105	148606	1.53
PC 5 US	392314	194513	2.02

Nomenclature: PC - PMMA/Cloisite 30B nanocomposite, US - nanocomposite synthesized with sonication, MS - nanocomposite synthesized with mechanical stirring, 1, 2 and 5 - clay loading in wt% during synthesis of nanocomposite

sized with sonication had a weight average molecular weight (M_w) of 435,392 g mol^{-1}, whereas nanocomposites synthesized using sonication showed significant increase in M_w, i.e., 478,506 and 581,130, which is approximately 10 and 33.5% higher for 1 and 2 wt% clay loading, respectively. This result is explained as follows: application of sonication during emulsion polymerization increases generation of free radicals in reaction volume. In this case, radicals form not only from the dissociation of the inorganic initiators at high temperature, but also from thermal dissociation of vapor entrapped in cavitation bubble during transient collapse. This combined source of radicals can increase the polymerization rate, resulting in rise of molecular weight of the resultant nanocomposite. A notable result is that molecular weights of nanocomposites synthesized with sonication are larger than the molecular weights of nanocomposites synthesized with mechanical stirring for same clay loading. This result is also attributed to exfoliation of the clay tactoids, increase in the interlayer *d*-spacing of clay and uniform dispersion of the platelets in polymer matrix due to intense microturbulence generated by sonication [45,46]. This enhances the net surface area of the clay platelets, which can form sites for adsorption of monomer molecules leading to faster and better polymerization. Intense microturbulence also causes fine emulsification between organic (monomer) and aqueous (water) phases, and efficient transfer of radicals generated in aqueous phase to the organic phase, which leads to uniform polymerization all over reaction volume. Biggs and Grieser [47] also emphasized the role of sonication towards achieving faster polymerization rates and higher molecular weight of polymers via generation of free radicals followed by formation of small latex particle size. On the other hand, in conventional emulsion polymerization with mechanical stirring, exfoliation of clay tactoids does not occur. Moreover, due to rather coarse emulsification, the interfacial area between organic and aqueous phase is limited, and transfer of radicals across phases does not occur effectively. The clay does get uniformly dispersed in reaction volume and can, in fact, hinder the mass transfer. This results in non-uniform polymerization over the reaction volume leading to smaller molecular weights of the nanocomposites.

CONCLUSIONS

Rheological and mechanical properties of PMMA/Cloisite 30B nanocomposites synthesized with ultrasound-assisted in-situ emulsion polymerization were investigated. Application of sonication during emulsion polymerization caused complete exfoliation of clay tactoids, with uniform dispersion in polymer matrix. The incorporation of nanoclay platelets into PMMA matrix significantly improved the bulk and storage modulus of the resulting nanocomposites. Addition of clay in polymer matrix also increased the complex viscosity of nanocomposites, agreeing well with the viscoelastic behavior of the resulting nanocomposites. Largest Young's modulus of nanocomposites was obtained for 2 wt% clay loading. The molecular weight of nanocomposites synthesized with sonication was also higher than pristine PMMA. In summary, ultrasound assisted emulsion polymerization can be an effective method for synthesis of PMMA/Cloisite 30B nanocomposites with high rheological and mechanical properties.

ACKNOWLEDGEMENT

The authors would like to acknowledge the Department of Science and Technology (Govt of India) for the FIST Grant No. SR/FST/ETII-028/2010. Authors also acknowledge the following for different analytical facilities: (1) Central Instruments Facility (CIF), I.I.T. Guwahati; (2) Dept of Mechanical Engineering I.I.T. Guwahati; (3) North Eastern Hill University, Shillong, and (4) CoE-SUSPOL, I.I.T. Guwahati.

NOMENCLATURE

G' : storage modulus [Pa]
G'' : loss modulus [Pa]
$G(t)$: relaxation modulus at time
M_w : weight average molecular weight [g/mol]
M_n : number average molecular weight [g/mol]
η^* : complex viscosity [Pa s]
ω : angular velocity [rad/s]

REFERENCES

1. L. J. Borthakur, D. Das and S. K. Dolui, *Mater. Chem. Phys.*, **124**, 1182 (2010).
2. A. B. Morgan and J. D. Harris, *Polymer*, **45**, 8695 (2004).
3. N. Moussaif and G. Groeninckx, *Polymer*, **44**, 7899 (2003).
4. Y. Xu, W. J. Brittain, R. A. Vaia and G. Price, *Polymer*, **47**, 4564 (2006).
5. P. Maiti, P. H. Nam, M. Okamoto, T. Kotaka, N. Gasegawa and A. Usuki, *Macromolecules*, **35**, 2042 (2002).
6. J. W. Gilman, *Appl. Clay Sci.*, **15**, 31 (1999).
7. S. Sharma, M. K. Poddar and V. S. Moholkar, *Ultrason. Sonochem.*, **36**, 212 (2017).
8. M. J. Solomon, A. S. Almusallam, K. F. Seefeldt, A. Somwangthanaroj and P. Varadan, *Macromolecules*, **34**, 1864 (2001).
9. M. Alexandre and P. Dubois, *Mater. Sci. Eng.*, **28**, 1 (2000).
10. M. K. Poddar, S. Sharma and V. S. Moholkar, *Macrolmol. Symp.*, **361**, 82 (2016).
11. H. T. Jung, S. S. Lee, M. Park, H. Kim and S. Lim, *Compos. Interfaces.*, **19**, 565 (2012).
12. M. K. Poddar, S. Sharma and V. S. Moholkar, *Polymer*, **99**, 453 (2016).
13. X. Huang and W. J. Brittain, *Macromolecules*, **34** (10), 3255 (2001).
14. G. A. Wang, C. C. Wang and C. Y. Chen, *Polymer*, **46**, 5065 (2005).
15. S. V. Krishna and G. Pugazhenthi, *Int. J. Polym. Mater.*, **60**, 144 (2010).
16. B. Zidelkheir, S. Boudjemaa, M. A. Goad and B. Djellouli, *Iran. Polym. J.*, **15**, 645 (2006).
17. M. K. Poddar, S. Pradhan, V. S. Moholkar, M. Arjmand and U. Sundararaj, *AIChE J.*, **64**, 673 (2018).
18. O. Yilmaz, C. N. Cheaburu, D. Durraccio, G. Gulumser and C. Vasile, *Appl. Clay Sci.*, **49**, 288 (2010).
19. Y. Q. Zhang, J. H. Lee, J. M. Rhee and K. Y. Rhee, *Compos. Sci. Technol.*, **64**, 1383 (2004).
20. M. K. Chang and H. C. Lee, *Int. Commn. Heat. Mass.*, **67**, 21 (2015).
21. K. Buruga and T. K. Jagannathan, *Mater. Today -Proc.*, **4**, 7467

(2017).
22. S. K. Patra, G. Prusty and S. K. Swain, *Bull. Mater. Sci.*, **35**, 27 (2012).
23. Z. Cherifi, B. Boukoussa, A. Zaoui, M. Belbachir and R. Meghabar *Ultrason. Sonochem.*, **48**, 188 (2018).
24. M. K. Poddar, M. Arjmand, U. Sundararaj and V. S. Moholkar, *Ultrason. Sonochem.*, **43**, 38 (2018).
25. B. A. Bhanvase, D. V. Pinjari, P. R. Gogate, S. H. Sonawane and A. B. Pandit, *Chem. Eng. J.*, **181**, 770 (2012).
26. B. A. Bhanvase and S. H. Sonawane, *Chem. Eng. J.*, **156**, 177 (2010).
27. K. S. Suslick, *Sonochemistry, Sci.*, **247**, 1439 (1990).
28. R. Kuppa and V. S. Moholkar, *Ultrason. Sonochem.*, **17**, 123 (2010).
29. Y. T. Shah, A. B. Pandit and V. S. Moholkar, Plenum Press, New York, (1999).
30. M. Ashokkumar and T. Mason, John Wiley & Sons (2007).
31. A. Kotronarou, G. Mills and M. R. Hoffmann, *J. Phys. Chem.*, **95**, 3630 (1991).
32. M. Sivakumar, A. Towata, K. Yasui, T. Tuziuti and Y. Iida, *Curr. Appl. Phys.*, **6**, 591 (2006).
33. S. Chakraborty, M. Kumar, K. Suresh and G. Pugazhenthi, *Powder Technol.*, **256**, 196 (2016).
34. M. Kumar, N. Shanmuga Priya, S. Kanagaraj and G. Pugazhenthi, *Nanocomposites*, **2**, 109 (2016).
35. J. G. Ryu, S. W. Park, H.-Kim and J. W. Lee, *Mater. Sci. Eng.*, **24**, 285 (2004).
36. J. Peanasky, L. L. Cai, S. Granick and C. R. Kessel, *Langmuir*, **10**, 3874 (1994).
37. S. Granick and H. W. Hu, *Science*, **258**, 1339 (1992).
38. F. R. Schwarzl, *Rheol. Acta*, **14**, 581 (1975).
39. B. J. Park, T. H. Kim, H. J. Choi and J. H. Lee, *J. Macromol. Sci. B*, **46**, 341 (2007).
40. D. S. Jang and H. J. Choi, *Colloid Surf., A*, **469**, 20 (2015).
41. C. A. Mitchell, J. L. Bahr, S. Arepalli, J. M Tour and R. Krishnamoorti, *Macromolecules*, **35**, 8825 (2002).
42. N. Moussaif and G. Groeninckx, *Polymer*, **44**, 7899 (2003).
43. S. K. Swain and A. I. Isayev, *Polymer*, **48**, 281 (2007).
44. M. Kumar, S. Arun, P. Upadhyaya and G. Pugazhenthi, *I.J.M.M.E.*, **10**, 1 (2015).
45. S. T. Lim, H. J. Choi and M. S. Jhon, *J. Ind. Eng. Chem.*, **9**, 51 (2003).
46. S. K. Lim, J. W. Kim, I. J. Chin and H. J. Choi, *J. Appl. Polym. Sci.*, **86**, 3735 (2002).
47. S. Biggs and F. Grieser, *Macromolecules*, **28**, 4877 (1995).